





RESEARCH ARTICLE OPEN ACCESS

Erythrocyte Extracellular Vesicles Amalgamate into the Hair and Skin to Maintain Homeostasis

Zeyuan Cao¹  | Peiyi Li¹ | Manjin Zhang²  | Simin Cai¹ | Na Li³ | Mingtao Luo³ | Yinghui Li⁴ | Haolin Wu⁵ | Xueli Mao¹  | Ruibao Ren⁵ | Hongju Xie³ | Songtao Shi^{1,5} 

¹Hospital of Stomatology, Guanghua School of Stomatology, Sun Yat-sen University, South China Center of Craniofacial Stem Cell Research, Guangdong Provincial Key Laboratory of Stomatology, Guangzhou, China | ²Stomatological Hospital, School of Stomatology, Southern Medical University, Guangzhou, China | ³Department of Plastic Surgery, the Second Affiliated Hospital of Hainan Medical University, Haikou, China | ⁴Department of Orthodontics, Hospital of Stomatology, Hebei Medical University, Shijiazhuang, China | ⁵International Center for Aging and Cancer, Hainan Medical University, Haikou, China

Correspondence: Hongju Xie (XieHJ@hainmc.edu.cn) | Songtao Shi (shisongtao@mail.sysu.edu.cn)

Received: 14 September 2024 | **Accepted:** 28 March 2025

Funding: This work was supported by grants from the National Key Research and Development Program of China (2021YFA1100600 to S.S., 2022YFA104402 to X.M.), Pearl River Talent Recruitment Program (2019ZT08Y485, 2019JC01Y182 to S.S.), Hainan Health and Medical Technology Innovation Joint Project (WSJK2024MS152 to H.X.) and Hainan Provincial Higher Education Scientific Research Project (Hnky2021ZD-16 to H.X.).

Keywords: erythrocytes | extracellular vesicles | hair | regeneration | skin

ABSTRACT

Erythrocytes are a major cell type in the circulation, numbering between 20 and 30 trillion. The function of erythrocytes is to bring oxygen to the tissues and release carbon dioxide to the lungs. Anaemic patients, who have low levels of erythrocytes, show significant symptoms affecting the hair and skin; however, the detailed relationship between erythrocytes and the integumentary system is not fully understood. Here, we show that erythrocyte extracellular vesicle (EV) can transfer haemoglobin, ABO antigens and keratin into the hair and promote hair regeneration through miR-20a-5p- and miR-22-3p-mediated upregulation of Wnt/ β -catenin signalling in dermal papilla cells. Moreover, we show that local injection of autologous erythrocyte EVs ameliorates hair growth in androgenic alopecia (AGA) patients. Interestingly, we found that erythrocyte EVs exit the body from the hair/skin and their membranes contribute to the formation of the outer barrier of the skin. In summary, we identify a previously unknown role of erythrocytes in amalgamating into hair structures and reveal a new therapeutic approach using erythrocyte EVs to promote hair regeneration in AGA patients.

1 | Introduction

The total number of cells in the whole human body is calculated to be about 3.72×10^{13} , of which the erythrocytes (red blood cells) comprise the largest population, numbering between 20 and 30 trillion, account for 70% of the cells in the body (Bianconi et al. 2013; Sender et al. 2016). Mature erythrocytes do not have nuclei or organelles such as mitochondria or ribosomes. For this reason, erythrocytes may be considered as highly specialised large extracellular vesicles (EVs) with enriched haemoglobin (Pasini

et al. 2010). Erythrocyte EVs contain erythrocyte-specific proteins such as haemoglobin, band 3 and glycophorin A (CD235a), as well as abundant lipid molecules including cholesterol, phosphatidylserine, ceramide (Cer) and various microRNAs (miRNAs) (Thangaraju et al. 2020). However, the detailed biological metabolism and characteristics of endogenous erythrocyte EVs are not fully understood.

Erythrocytes play a vital role in transporting oxygen, glucose and electrolyte contents through the circulation to all portions

This is an open access article under the terms of the [Creative Commons Attribution-NonCommercial-NoDerivs](https://creativecommons.org/licenses/by-nc-nd/4.0/) License, which permits use and distribution in any medium, provided the original work is properly cited, the use is non-commercial and no modifications or adaptations are made.

© 2025 The Author(s). *Journal of Extracellular Vesicles* published by Wiley Periodicals LLC on behalf of International Society for Extracellular Vesicles.

of the body. They also carry away carbon dioxide and other waste products. Under physiological and pathological conditions, erythrocyte EVs play critical roles in the maintenance of nitric oxide homeostasis, redox balance, immunomodulation and coagulation (Thangaraju et al. 2020). Recently, it was reported that erythrocytes play additional biological functional roles, such as modulating innate immunity, binding chemokines and nucleic acids, and controlling invading pathogens (Lam et al. 2021).

An organ system is a group of organs that work together in the body to perform a complex function. The human body has 11 organ systems to maintain the body's normal activities. Recent studies show that organ systems communicate using multiple biological pathways such as a variety of signalling mechanisms mediated by hormones, cytokines and growth factors (Castillo-Armengol et al. 2019; Herrlich et al. 2022). EVs can serve as vehicles to transfer cargos between organs (Armutcu 2019). The circulatory system's main function is to move blood throughout the body. This system's primary components are the heart, lungs, veins and arterial vessels through which blood travels. The integumentary system consists of the skin, nails, hair and glands on the outside of the body, forming a crucial physical barrier against bodily intrusion by infectious agents, penetrating objectives and UV radiation (Grubauer et al. 1987; Harris-Tryon and Grice 2022). Anaemia is haematological state characterised by a low-erythrocyte counts and low-haemoglobin level. The majority of anaemic patients present with pale, dry and rough skin as well as damaged hair and moderate alopecia (Lopez et al. 2016). It is believed that anaemia-induced hair damage may be due to reduced supply of oxygen and iron to the hair follicles. Although it has been speculated that erythrocytes closely interplay with the integumentary system, the detailed relationship between erythrocytes and hair/skin is largely unknown. Androgenic alopecia (AGA) is a common hair loss disorder, with up to 80% of men and 50% of women affected (Piraccini and Alessandrini 2014). Only 5- α reductase inhibitors and minoxidil are available therapies for AGA (Saceda-Corralo et al. 2023; Varothai and Bergfeld 2014), it is necessary to develop more effective and convenient therapeutic approach for AGA.

In this study, we show that erythrocyte EVs can be converted to integumentary elements, making important contributions to structures of the hair and skin. Erythrocyte EVs participate in hair and skin metabolism and promote hair growth in AGA patients, suggesting a new approach to use erythrocyte EVs for hair regeneration.

2 | Materials and Methods

2.1 | Erythrocytes and Isolation of Erythrocyte EVs

Mouse erythrocyte EVs were prepared according to the protocol reported previously (Vorselen et al. 2018). Whole blood was collected in EDTA tubes and mixed with equal volume of saline. Erythrocytes were separated by density gradient centrifugation using a red blood cell isolation kit (TBDscience Tech Co., LTD). Then, separated erythrocytes were washed with saline and resuspended in Ringer's buffer (32 mM HEPES, 125 mM NaCl, 5 mM KCl, 1 mM MgSO_4 , 1 mM CaCl_2 , 5 mM glucose, pH 7.4).

Erythrocytes were stimulated with 4 μM Ca^{2+} ionophore (MCE) for 6 h at 37°C. To purify EVs, erythrocytes and cell debris were removed by centrifugation at 800 \times g for 10 min at 4°C and 2000 \times g for 10 min at 4°C. The supernatants were passed through 0.45 μm syringe filters. EVs were centrifuged and concentrated at 20,000 \times g for 30 min at 4°C.

For labelling, erythrocyte EVs were stained with PKH26 (Sigma-Aldrich), PKH67 (Sigma-Aldrich), Ter-119 (Biolegend, #116212, APC antimouse) or MemGlow 640 Fluorogenic Membrane Probe (Cytoskeleton). For PKH26 or PKH67 labelling, EV pellets were resuspended in 100 μL of Dilution C solution at a concentration of 1×10^{12} particles/mL, and then 1 μL of PKH26 or PKH67 dye diluted by 100 μL of Dilution C solution was added. The mixture was incubated at room temperature for 5 min, followed by the addition of an equal volume of 5% bovine serum albumin (BSA)/phosphate buffered saline (PBS) solution to block the excess dye. The mixture was then centrifuged again at 20,000 \times g, 4°C for 30 min to remove any excess dye and washed once in PBS buffer. For Ter-119 labelling, EVs were resuspended in PBS buffer at a concentration of 1×10^{12} particles/mL. Then, every 100 μL of EV solution was mixed with 1 μL of Ter-119 antibody and incubated at room temperature for 30 min. After staining, the mixture was centrifuged at 20,000 \times g, 4°C for 30 min to collected EVs and subsequently washed once in PBS buffer. For MemGlow labelling, EVs were resuspended in PBS buffer at a concentration of 1×10^{12} particles/mL. Then, every 100 μL of EV solution was mixed with 2 μM MemGlow probe diluted in 100 μL of PBS and incubated at room temperature for 10 min. After staining, the mixture was centrifuged at 20,000 \times g, 4°C for 30 min to collected EVs and subsequently washed once in PBS buffer. Human blood samples were obtained from healthy donors with informed consent. All experiments with human blood samples were performed according to the guidelines and the approval of the Medical Ethics Committee of Hospital of Stomatology, Sun Yat-sen University (KQEC-2023-31-02).

2.2 | Erythrocyte EV Characterisation

The concentration, average particle size and Zeta potential of erythrocyte EVs were measured using ZetaView PMX120 (Particle Metrix). Experimental data was analysed using ZetaView analysis software (Version 8.02.31) with a minimum size of 10 nm, a maximum size of 5000 nm and a minimum brightness of 30 nm. The ferrous (Fe^{2+}) and ferric (Fe^{3+}) iron in mouse erythrocyte EVs were quantified by Iron Assay Kit (abcam), according to the manufacturer's protocol, and shown by Prussian blue reaction (solarbio).

2.3 | Animal Experiments

C57BL/6 mice and Balb/c mice (half male and half female, 7 weeks old, 18–22 g) were purchased from GuangDong Gem Pharmatech. KRT14-RFP mice were kindly provided by Dr. Li Ji of Central South University (Changsha, China). All animal experiments were compliant with the ethics committees of Sun Yat-sen University (SYSU-IACUC-2022-001802, SYSU-IACUC-2023-001256).

To generate anaemia model, mice were injected intraperitoneally twice a week for 3 weeks with acetylphenyl hydrazine (APH, 60 mg/kg, Meilun Biotechnology), a potent oxidant that has specific and progressive oxidative damage on haemoglobin, resulting in erythrocyte destruction (haemolysis) and causing haemolytic anaemia. The counts of erythrocytes and haemoglobin were monitored for 3 weeks. The activity of the mice as well as their mental status and appearance of skin and hair were monitored every day. For EV treatment, erythrocyte EVs (2×10^{11} particles in 200 μ L PBS per mouse) or PBS (200 μ L) as a control were injected subcutaneously into the dorsum of mice twice a week for 2 weeks. All mice were sacrificed at scheduled time points to collect hair and skin samples for further analysis.

For hair regeneration, dorsal skin hairs in the telogen phase from 7-week-old C57BL/6 and Balb/c mice were depilated with a mechanical trimmer and depilatory cream. Erythrocyte EVs (2×10^{11} in 200 μ L PBS per mouse) or PBS (200 μ L) as a control were injected subcutaneously into the dorsum of mice twice a week for 2 weeks. 5% Minoxidil (TCI) was topically applied twice a week for 2 weeks to the dorsal skin as a positive control. Images of each mouse were captured after 0, 3, 7, 10 and 14 days, and the level of pigmentation was quantified by the darkness intensity of the back colour in the same area using ImageJ software. All mice were sacrificed at scheduled time points to collect blood, hair and skin samples for further analysis.

2.4 | Ex Vivo Erythrocyte EV Distribution

Three 7-week-old wildtype mice were allocated to each group for EV distribution study. PKH26-labelled erythrocyte EVs (5×10^{11} particles in 200 μ L PBS per mouse) were injected into wildtype mice through the tail vein. 5 μ L of PKH26 dye diluted in equal volume of PBS buffer was used as negative control. After injection for 7 days, the biodistribution of erythrocytes or erythrocyte EVs in the heart, liver, spleen, lung, kidney and skin tissues was imaged with Xenogen IVIS 100 (PerkinElmer). The fluorescence intensity was quantified with Living Image software (PerkinElmer). After injection for 1, 3 and 7 days, hair and skin tissues were collected and prepared for immunofluorescent staining. The distribution pattern of erythrocytes or erythrocyte EVs in skin and hair was further observed by LSM 980 (Zeiss) after immunofluorescent staining. In addition, Ter-119 or MemGlow labelled-erythrocyte EVs (5×10^{11} particles in 200 μ L PBS per mouse) were also injected to verify the distribution characteristics of erythrocyte EVs in the skin.

2.5 | Dermal Papilla Cell (DPC) and Skin-Derived Mesenchymal Stem Cell (SMSC) Isolation and Culture

Dermal papillae (DPs) and skin tissues were isolated and collected from 4-week-old C57BL/6J mice. The lip pads containing vibrissae were excised using scissors and immersed in cold PBS. Under a dissecting microscope, forceps and scissors were used to remove the subcutaneous fat and connective tissue to expose the root of vibrissae. Individual vibrissae were carefully isolated by gently pulling them away from the pad. The matrix component and any epithelial tissue still present on the papilla were teased off. The

end bulb and skin tissues were then dissected and digested with solution containing Collagenase Type I (1 mg/mL, Worthington Biochemical) and Dispase II (1 mg/mL, Roche Diagnostics) in PBS for 30 min at 37°C. Extracted papillae and skin tissues were seeded into 6-cm dishes and cultured in MEM Alpha basic (α -MEM, Thermo Fisher) with 10% foetal bovine serum (FBS, ExCell Bio) and 1% penicillin/streptomycin (Invitrogen). Colony-forming attached cells were collected and passed for further experimental use.

2.6 | Dynamic Migration of Erythrocyte EVs Detected by IVIM

Eight-week-old KRT14-RFP mice were anaesthetised with intraperitoneal injection of ketamine and xylazine, and the skin around the dorsal region was prepared by shaving with a mechanical trimmer and depilatory cream. PKH67-labelled erythrocyte EVs (5×10^{11} particles in 200 μ L PBS per mouse) were intravenously injected into the mouse, administered 3 days before imaging. The detected area was immobilised by a vacuum extractor and imaged directly under a water lens. Image stacks of the skin were acquired with an intravital fluorescence microscopy (IVIM) equipped with a two-photon laser. Serial optical sections were acquired to image the layer of stratum corneum (SC) at 2 min intervals for a total of 60 min.

2.7 | Scanning Electron Microscopy (SEM)

Hair shafts were collected from the same site on the mouse abdomen or dorsum. The prepared hair was fixed onto the specimen stub, and then gold coating was applied to the fixed hair by a sputter coating machine. The hair was inserted into the scanning electron microscope (QUANTA 200, 30 kV, FEI) for viewing and photography.

2.8 | Transmission Electron Microscopy (TEM)

Erythrocyte EVs were diluted in acetone and dispersed by ultrasonic oscillation for 15 min, then the dispersion solution was dropped onto carbon-coated copper grids and dried at room temperature. The TEM images were captured by TEM 120 kV (Tecnai G2 Spirit, FEI, USA).

2.9 | H&E Staining

Mouse heart, liver, spleen, lung, kidney and skin tissues were fixed with 4% paraformaldehyde (PFA, Servicebio). The paraffin-embedded sections (6 μ m) were prepared for H&E staining. The images were obtained by optical microscopy (Zeiss). The number and growth state of hair follicles were analysed by ImageJ software.

2.10 | Immunofluorescent Staining

Hair and skin tissues were collected and fixed in 4% PFA after injection of labelled mouse or human erythrocyte EVs through

the tail vein. The frozen sections (6 μm) were prepared for immunofluorescent staining. First, the sections were washed with PBS and blocked with 5% (w/v) BSA for 1 h at room temperature. Then, the sections were incubated with primary antibodies specific for haemoglobin subunit alpha (HBA, Affinity Biosciences), haemoglobin subunit beta (HBB, Affinity Biosciences), Krt14 (Invitrogen), or active β -catenin (Merck) for 4 h at room temperature. After washing with PBS, the sections were incubated with secondary antibodies conjugated to Alexa647 (Invitrogen, Carlsbad, CA) for 1 h at room temperature. Last, the cytoskeleton and nucleus were stained with ActinGreen 488 (Invitrogen) and Hoechst 33342 (0.1 $\mu\text{g}/\text{mL}$, Invitrogen), respectively. Fluorescent images were observed and recorded by LSM 980 (Zeiss).

2.11 | Immunohistochemical Staining

The immunohistochemical staining of hair was performed according to an immunohistochemistry kit (Elabscience). Briefly, to block endogenous peroxidase activity, the frozen sections (6 μm) were incubated in 3% H_2O_2 for 10 min at room temperature. Then, the sections were blocked with goat blocking buffer for 30 min at 37°C and incubated with primary antibodies specific for human ABO antigen (Elabscience) for 2 h at room temperature. After washing with PBS, the sections were incubated with polyperoxidase-anti-Mouse/Rabbit IgG for 30 min at 37°C. Finally, the sections were stained with DAB working buffer and washed with ddH_2O until they showed light brown staining.

2.12 | Proteomic Analysis

Mice were systematic infusion with human erythrocyte EVs (2×10^{14} particles in 200 μL saline) twice a week through the tail vein injection. After 1 month, the hair shaft was cut off at the mouse skin surface using surgical scissors without damaging the skin. Proteins were extracted, identified and analysed by Bionovogene Co. Ltd. (Suzhou, China). Briefly, the samples were ground into powder in liquid nitrogen and dissolved in lysis buffer. After removing debris by centrifugation at $14,000 \times g$ at 4°C for 20 min, the supernatant was collected, and the protein concentration was determined with a BCA kit (Thermo Fisher) according to the manufacturer's instructions.

For trypsin digestion, the extracted hair protein solution was reduced with 5 mM dithiothreitol for 1 h at 37°C and alkylated with 10 mM iodoacetamide for 45 min at room temperature in darkness. The protein sample was then diluted four times by adding 25 mM ammonium bicarbonate. Finally, trypsin was added at a 1:50 trypsin-to-protein mass ratio for the first digestion overnight at 37°C.

After trypsin digestion, the peptides were desalted by XBridge Strata X C18 SPE column (Phenomenex) and vacuum dried. TMT reagent (Thermo Fisher Scientific) was thawed and reconstituted in acetonitrile. Peptides were reconstituted in 0.5 M TEAB and processed according to the manufacturer's protocol for TMT16plex Isobaric Label Reagent Set (Thermo Fisher). The peptide mixtures were then incubated for 1 h at room temperature and pooled, desalted and dried by vacuum centrifugation.

The tryptic peptides were fractionated by high pH reverse-phase HPLC using XBridge Peptide BEH C18 column (5 μm , waters). The raw data generated from a high-resolution mass spectrometer were processed and quantified by Proteome Discoverer software v2.4.1.15 (Thermo Fisher), and searched against the (RefSeq Human protein database [24078 sequences, release 2017_03]) using the SEQUEST algorithm. Student's *t* test was used to identify proteins with significantly different expression (Fold change > 1.2 and *p* value < 0.05). Proteins were classified by Gene Ontology (GO) (<http://david.abcc.ncifcrf.gov/home.jsp>) annotation based on three categories: biological process (BP), cell component (CC) and molecular function (MF). The Kyoto Encyclopedia of Genes and Genomes (KEGG) database (<http://www.genome.jp/kegg/>) was used to annotate protein pathways. Based on the quantitative results, the differential expressed proteins between comparison groups were identified for functional enrichment and subcellular localisation analysis.

2.13 | Lipid Content Detection

To quantify the lipid content within mouse erythrocyte EVs, a total of 5×10^{11} EVs were isolated and prepared for analysis. To compare the lipid content within mouse SC after EV injection, six of 7-week-old C57BL/6 mice were injected intravenously with mouse erythrocyte EVs (5×10^{11} particles in 200 μL PBS per mouse) in EV group. Three mice were injected intravenously with equal volume PBS buffer as control. After injecting for 7 days, dorsal skin hairs in the telogen phase were depilated. The bare skin was washed gently with ddH_2O and allowed to dry naturally at room temperature. Lipids within SC were collected from two sampling sites on the dorsal skin. The lipids were collected using a D-Squame sampling disc (D100). A disc was pressed on the sampling site for 15 s with a D-Squame pressure instrument (D500) providing uniform pressure (225 g/cm^2), and removed with one fluid motion. Place another skin disc in the same sampling site and repeat the operation twice. Samples were placed into a tube and stored at -80°C until extraction.

Lipid contents were extracted and analysed by MetWare (<http://www.metware.cn/>) based on the AB Sciex QTRAP 6500 LC-MS/MS platform (Wuhan, China). For extraction, a sample was removed from the -80°C refrigerator and thawed on ice. Then 1500 μL of the extraction solvent (methyl *tert*-butyl ether:methanol = 3:1, v/v) containing internal standard mixture was added to two pieces of the sample. After whirling the mixture for 15 min, 300 μL of ultrapure water was added. The mixture was then vortexed for 1 min and centrifuged at $12,000 \times g$ for 10 min. 1000 μL of the upper organic layer was collected and evaporated using a vacuum concentrator. The dry extract was reconstituted using 200 μL mobile Phase B before LC-MS/MS analysis. The sample extracts were analysed using an LC-ESI-MS/MS system (UPLC, ExionLC AD, <https://sciex.com.cn/>; MS, QTRAP 6500+ System, <https://sciex.com/>). LIT and triple quadrupole (QQQ) scans were acquired on a triple quadrupole-linear ion trap mass spectrometer (QTRAP), QTRAP 6500+ LC-MS/MS System, equipped with an ESI Turbo Ion-Spray interface, operating in positive and negative ion mode and controlled by Analyst 1.6.3 software (Sciex).

Differentially regulated metabolites between groups were determined by VIP ($VIP \geq 1$) and absolute \log_2FC ($|\log_2FC| \geq 1.0$). Identified metabolites were annotated using KEGG Compound database (<http://www.kegg.jp/kegg/compound/>), annotated metabolites were then mapped to KEGG Pathway database (<http://www.kegg.jp/kegg/pathway.html>).

2.14 | MALDI-TOF-MS

Cryosections of the mouse skin tissues were cut in a cryomicrotome at a thickness of 10 μm and transferred onto conductive indium-tin-oxide-coated glass slides for MALDI imaging (Bruker). Before detection, the slides were placed in a vacuum dryer for 5 min, washed by 70% and 96% ethanol and dried in a vacuum dryer again. The sections were coated with matrix using an ImagePrep (Bruker Daltonik) according to the manufacturer's standard protocols. Lipid detection was performed in the mass range of 140–1200 m/z . The mouse skin dataset was acquired at a lateral resolution of 100 μm . For each pixel, 200 laser shots were accumulated at constant laser energy. All data were analysed by SCI LS Lab software (Version 2016b/Release 4.1, Bruker).

2.15 | Western Blotting

Cells or EVs were harvested and lysed in RIPA (Santa Cruz Biotechnology) on ice for 30 min. Total protein concentrations were measured by a BCA protein assay kit (Invitrogen). Western blotting assay was performed using protocols described below. Briefly, total protein (30 μg) was loaded onto NuPAGE Bis-Tris gel (Invitrogen) and transferred to polyvinylidene fluoride (PVDF) membranes (Millipore). The membranes were blocked for 1 h at room temperature, then incubated at 4°C overnight with antibodies against HBA (Affinity Biosciences), HBB (Affinity Biosciences), Axin2 (Cell Signaling Technology), β -catenin (Merck), active β -catenin (Merck), Alix (abcam), TSG101 (abcam), CD9 (abcam), CD63 (Santa Cruz), CD81 (Santa Cruz) or β -actin (Sigma). After washing with Tris buffered saline (TBS) containing 0.1% Tween-20, the membranes were incubated with species-related peroxidase-conjugated secondary antibodies for 1 h at room temperature. The protein bands were visualised using SuperSignal West Pico PLUS Chemiluminescent Substrate kit (Thermo Fisher) and SuperSignal West Femto Maximum Sensitivity Substrate kit (Invitrogen), and detected by a ChemiDoc MP imaging system (Bio-Rad).

2.16 | Cell Counting Kit-8 Assay

Cells were seeded into 96-well plates (2000 cells per well) and cultured in medium without or with erythrocyte EVs ($1 \times 10^{11}/\text{mL}$) for 3 days. The cell proliferation rate was detected by using a Cell Counting Kit-8 (CCK-8, Dojindo) according to the manufacturer's instructions. The optical density (OD) value at 450 nm was detected using a Synergy H1 Hybrid Multi-Mode Reader (BioTek).

2.17 | Osteogenic Differentiation and Alizarin Red Staining

For osteogenic differentiation, cells were seeded onto 12-well plates (3×10^4 cells per well) for 3 days, followed by induction with osteogenic differentiation medium (α -MEM that containing 10% FBS, 2 mM β -glycerophosphate [Sigma], 10 nM dexamethasone [Sigma] and 100 μM L-ascorbic acid 2-phosphate [Sigma]) for 14 days. For alizarin red staining, cells were fixed with 4% PFA and stained with 1% (w/v) alizarin red staining solution (Sigma) for 10 min at room temperature. Then, the cells were washed with PBS and observed under an optical microscope (Zeiss). The colour depth of alizarin red was analysed by ImageJ software.

2.18 | Adipogenic Differentiation and Oil Red O Staining

For adipogenic differentiation, cells were seeded onto 12-well plates (3×10^4 cells per well). When the cells reached 100% confluence and stopped proliferating, they were induced with adipogenic medium containing 500 nM hydrocortisone (Sigma), 500 nM isobutylmethylxanthine (Sigma), 100 nM L-ascorbic acid phosphate, 10 $\mu\text{g}/\text{mL}$ insulin (Sigma) and 60 μM indomethacin (Sigma) for 14 days. For oil red O staining, the lipid droplets in cells were stained with oil red O solution (Sigma) for 15 min at room temperature. The density of the lipid droplets was observed under an optical microscope (Zeiss) and analysed by ImageJ software.

2.19 | miRNAs Transfection and RT-qPCR

miRNA mimics and inhibitors were synthesised by Tsingke Biotech Co., Ltd. (Beijing, China). miR-20a-5p, miR-22-3p and miR-195a-5p mimics were transfected in DPCs using RNAiMAX agent (Invitrogen) and incubated for 24 h. Inhibitors of miR-20a-5p and miR-22-3p were transfected in erythrocytes using RNAiMAX agent and incubated for 12 h. Total RNA of cells was isolated using the miRNeasy Mini Kit (Qiagen) and reverse transcribed into cDNA using Reverse Transcriptase M-MLV kit (TaKaRa) according to the manufacturer's instructions. RT-qPCR assay was performed according to the manufacturer's instructions of AceQ Universal SYBR qPCR Master Mix (Vazyme). U6 was used as the internal control. The expression level of targeted gene was analysed by $2^{-\Delta\Delta C_t}$ method.

2.20 | Dual-Luciferase Reporter Gene Assay

A fragment from the 3'-untranslated region (UTR) of Axin2 containing the putative binding sequences for miR-20a-5p or miR-22-3p was synthesised and cloned into a dual-luciferase vector pmirGLO (Table S1) (Tsingke Biotechnology). DPCs were plated in a 96-well culture plate at a density of 8000 cells/well. To verify Axin2 is the target gene of miR-20a-5p and miR-22-3p, DPCs in each well were transfected with 0.25 μg of miR-20a-pmirGLO, 0.25 μg of miR-22-pmirGLO vector, 0.25 μg of mutant vector or pmirGLO vector, using Hieff TransTM Liposomal Transfection Reagent (YEASEN). Then, cells were transfected with 25 nM of miR-20a-5p, miR-22-3p and NC mimics using

RNAiMAX agent. To demonstrate if the erythrocyte EVs can release miR-20a-5p and miR-22-3p, DPCs were transfected with 0.25 µg of miR-20a-pmirGLO, 0.25 µg of miR-22-pmirGLO vector, 0.25 µg of mutant vector or pmirGLO vector, and then incubated with erythrocyte EVs (1×10^{11} particles/mL). After transfection for 24 h, DPCs were washed once by PBS buffer and lysed on ice. Cell lysates were collected for further analysis. The firefly luciferase activity was measured and normalised to the Renilla luciferase activity, detected by Multi-Mode Reader (BioTek, USA).

2.21 | Erythrocyte EV Treatment for AGA Patients

The clinical trial was approved by the Second Affiliated Hospital of Hainan Medical University (IRB 2023-02-02) and registered in National Medical Research Registration and Filing Information System (www.medicalresearch.org.cn) (MR-46-24-032406). Written informed consents were obtained from all participants before enrollment. Eligible subjects included men between 18 and 60 years, who were diagnosed with AGA with at least M2, C2 or U1 basic type and V1 or F1 specific type of AGA, according to the Basic and Specific (BASP) classification (Lee et al. 2007). The specific inclusion and exclusion criteria were listed in Table S2.

For human autologous erythrocyte EV preparation, 20 mL of venous blood was collected from each subject. Blood was centrifuged at $800 \times g$, 4°C for 10 min, and then blood cells were collected for further separation. Erythrocytes collected from patients were separated by density gradient centrifugation using an erythrocyte isolation kit (TBDscience). Then, separated erythrocytes were washed with saline for three times and treated with an erythrocyte EV extraction kit (Beijing UUUD Technology Co., Ltd). To purify EVs, erythrocytes and cell debris were removed by centrifugation at $800 \times g$ for 10 min at 4°C and $2000 \times g$ for 10 min at 4°C. EVs were centrifuged and concentrated at $20,000 \times g$ for 30 min at 4°C. Collected EV pellets were washed with saline for three times and finally resuspended in 2 mL saline.

The method of EV administration was based on previous reports (Bruce et al. 2020; Kim et al. 2021). After local anaesthesia, patient's scalps were disinfected with chlorhexidine, and a grid was marked with dots approximately 1 cm apart, covering the 20 cm² treated area. A total of 2 mL of erythrocyte EVs ($4.88\text{--}6.71 \times 10^{12}$ particles/mL) were perpendicularly injected using a 34-gauge needle, approximately 0.1 mL per injection site and 20 injection points in the grid. The needle was angled close to 90°, targeting the transition between the dermis and subcutaneous layer. Erythrocyte EVs were injected into the scalp at 4 mm depth. Without removing immediately upon after injecting, the syringe was stuck in the scalp for approximately 2 s to prevent leakage of the injected EVs from the transplant site. After treatment, all subjects were required not to wash their hair on the day of EV injection and not to do excessive exercise for 1 week. Erythrocyte EV treatment was applied once every month for 3 months. Macroscopic and digital photos were taken at the beginning of each treatment (baseline), 1, 2, 3 and 6 months after the first treatment. All scalps were analysed by DermoScan Dermatoscope (DermoGenius ultra) in combination with TrichoScan digital image analysis (Trichoscan Automatic V 4.0). The data of nine subjects (Table S3) that finished three times erythrocyte EV injection and 6-month follow-up were presented in this study.

2.22 | Statistical Analysis

All experiments were performed in biological triplicate and data are expressed as mean \pm standard deviation (SD). Statistical and graph analysis were performed by GraphPad Prism 9. Multiple group comparisons were assessed by one-way ANOVA with Bonferroni test. For two-group comparisons, significance was analysed using independent unpaired or paired two-tailed Student's *t* tests. Values of $p < 0.05$ were considered statistically significant.

3 | Results

3.1 | Anaemic Mice Show Significant Hair and Skin Impairments

We established a chronic anaemia mouse model by APH induction to study the relationship between erythrocytes and integumentary hair/skin. Routine blood tests showed that the number of erythrocytes and haemoglobin content in anaemic mice were lower than that in control mice (Figure S1A). After 21 days of APH induction, all anaemic mice showed sluggish behaviour, tiredness, lack of lustre in the hair, and greying of the hair on the back and abdomen (Figure S1B). Visual observation of the organs showed splenomegaly, confirming successful generation of the anaemia mouse model (Figure S1C). H&E staining showed that the heart, liver, spleen and kidneys had observable histological abnormalities in anaemic mice (Figure S1D). For heart, the myocardial arrangement was disordered, the myocardial fibres were broken and the transverse lines disappeared. For liver, there were more lymphocyte infiltration and substantial deposition of haemosiderin particles. For spleen, the boundary between red pulp and white pulp was absent, with a large number of deposited haemosiderin particles. For kidney, there were also a large number of deposited haemosiderin particles, mainly involving renal tubules and renal tubule cells. Anaemic mice exhibited cracked and damaged hair cuticles with many fragments compared to the normal control group (Figure S1E). The overall thickness of the epidermal (EP) layer was thinner than that in the control, and the boundary between layers of the SC was disorganised in anaemic mice compared to control mice (Figure S1F). Almost all keratinocytes in the EP layer exhibited karyopyknosis with hyperchromatic nuclei in anaemic mice. The number of fibroblasts in the dermis of anaemic mice was significantly reduced (Figure S1F). Collectively, these results demonstrate that chronic anaemia can seriously impair integumentary hair and skin, resulting in the destruction of their physiological structure and function.

3.2 | Migration of Erythrocytes in the Integumentary Hair and Skin

To examine the relationship between erythrocytes and integumentary hair/skin, we tracked the migration of erythrocytes in vivo after the tail vein injection. Organ fluorescence imaging showed that the most of injected erythrocytes were distributed in the liver and skin, some were present in the lung, and a few were detected in the spleen and kidneys at 7 days after tail vein injection (Figure S2A). These data suggest that the skin may be

one of the main excretion sites of erythrocytes. Next, we examined the erythrocytes in the skin using super-resolution-structured illumination microscopy (SIM) and found that PKH26-labelled erythrocyte metabolites migrated to the dermis and epidermis after the tail vein injection (Figure 1A). The most of injected erythrocyte metabolites were distributed in the EP layer, hair and hair follicles, demonstrating that skin and hair may be an important elimination organ for erythrocytes (Figure 1A). Moreover, the fluorescent images showed that erythrocyte metabolites were distributed in the EP layer with vesicle-like structure at 3 days after injection. Some vesicle-like particles formed a linear aggregation on the surface of the EP layer (Figure 1B). Seven days after injection, almost all particles migrated to the surface of the EP layer and formed a thicker and banded structure on the EP layer (Figure 1B). We extracted PKH26-positived particles from the EP layer and found that they showed vesicle-like structure under SIM with average size about 182.1 nm assessed by nano-flow cytometry (NanoFCM) (Figure 1C), suggesting that erythrocytes may exit the body in the form of EVs. Collectively, these results indicate that the integumentary skin and hair are an excretion sites for erythrocytes.

3.3 | Characterisation of Mouse Erythrocyte EVs

To examine whether erythrocyte EVs can contribute to the integumentary system, we prepared and characterised mouse erythrocyte EVs using a calcium ionophore induction approach (Figure S2B). TEM analysis showed that erythrocyte EV presented a clear bilayer edge (Figure S2C). Zetaview results showed that each mouse erythrocyte produced around 205 EVs (Figure S2D), with an average particle size of 181.5 nm and Zeta potential of -33.89 ± 1.16 mV (Figure S2E). The ferrous (Fe^{2+}) and ferric (Fe^{3+}) iron in EVs were detected by Prussian blue reaction (Figure S2F, G). Western blotting results showed that erythrocyte EVs expressed general EV markers, such as Alix, TSG101, CD9, CD63 and CD81 (Figure S2H). The majority of mouse erythrocyte EVs also expressed Ter-119, a specific surface marker of mouse erythrocytes (Figure S2I).

3.4 | Migration of Erythrocyte EVs in the Integumentary Hair and Skin

Organ fluorescent images showed that erythrocyte EVs were mainly distributed in the skin (Figure 1D and Figure S2J). To investigate the movement of erythrocyte EVs during their excretion within living mice, we used IVIM to record the dynamic movement of PKH67-labelled erythrocyte EVs in the epidermis of KRT14-RFP mice after 3 days tail vein infusion. We confirmed that erythrocyte EVs dynamically migrated from the dermal layer to EP layer (Figure 1E). Over the time span from 20 to 60 min, an increasing number of EVs were observed moving from the interior of the skin to the surface (Figure 1F). It was a continuous process in which erythrocyte EV excretion was cooperated with EP renewal. The immunofluorescence staining further showed the migration pattern of erythrocyte EVs in the skin from 1 to 7 days after tail vein injection (Figure 1G, H). PKH26-labelled erythrocyte EVs gradually migrated from the basal layer to the EP layer over time, finally reached the surface of skin, and were ultimately shed (Figure 1G). Intravenous injection of only

PKH26 dye into mice was performed to exclude the potential dye artifacts (Figure S2K). This dynamic migration pattern was also observed in the skin injected with Ter-119- or MemGlow-labelled erythrocyte EVs (Figure 1G and Figure S2L). Next, we detected the distribution of erythrocyte EVs in the hair follicles and hair. After injection of erythrocyte EVs for 7 days, it was obvious that hair follicles entered into the anagen stage, and large quantities of erythrocyte EVs were taken up by the DP (Figure 1I). In addition, we showed that erythrocyte EVs were enriched in the sebaceous glands, integrated into hair shaft and the root of hair (Figure 1J). Extracted hair also showed that erythrocyte EVs migrated to the DP and participated in the structure of the hair shaft (Figure 1K). All these results demonstrate that erythrocyte EVs can integrate into the integumentary system, suggesting erythrocytes turn to hair/skin elements.

3.5 | Erythrocyte EVs Are Converted into Hair Components

Next, we showed that the specific components from erythrocyte EVs that take part in the formation of the integumentary system through proteomic analysis (Figure 2A). The results showed that one month after human erythrocyte EV intravenous injection, erythrocyte-specific proteins such as HBA1 and HBB were increased in the hair shafts of erythrocyte EV-infused mice (Figure 2B). Further, immunofluorescence images demonstrated that HBA of human origin was detected in the mouse hair shafts, becoming a part of the mouse fur after systematic infusion for 1 month (Figure 2C). It has been reported that A, B and H blood group substances can be detected in human hair medulla, which is a reliable method for determination of the ABO blood type in forensic medicine (Miyasaka et al. 1987; Nishi et al. 1989). Here, we showed that human A, B and H antigens were detectable in mouse hair cortex and medulla at 1 month after human erythrocyte EV injection (Figure 2D).

After matching with a mouse protein database and detecting by immunofluorescence staining, we further confirmed that mouse hair itself also contains haemoglobin subunits deposited in the matrix (Figure 2E and Figure S3A). The results showed that 115 mouse proteins were upregulated in the hair (Figure 2F). Among these, various kinds of keratins were significantly increased, such as keratin 1 (Krt1), keratin 10 (Krt10) and keratin 14 (Krt14) (Figure 2G and Figure S3B). According to the functional annotations in the GO database, these 115 upregulated proteins were derived from the cytoplasm, cornified envelope, keratin filament and cytoskeleton (Figure 2H) and played roles in some BPs, such as keratinisation, intermediate filament cytoskeleton organisation, cell division, actin filament organisation, cell differentiation and actin filament bundle assembly (Figure 2I). Furthermore, KEGG enrichment analysis revealed that these upregulated proteins in hair were associated with pathways pertaining to ribosomes, endocytosis, adhere junction, arachidonic acid metabolism and MAPK signalling (Figure S3C). We showed that haemoglobin subunits (HBB) accumulated at the EP layer and root of hair (Figure S3D, E), where some were colocalised with Krt14 (Figure S3E), suggesting that haemoglobin may participate in hair growth and keratinisation.

Figure 1

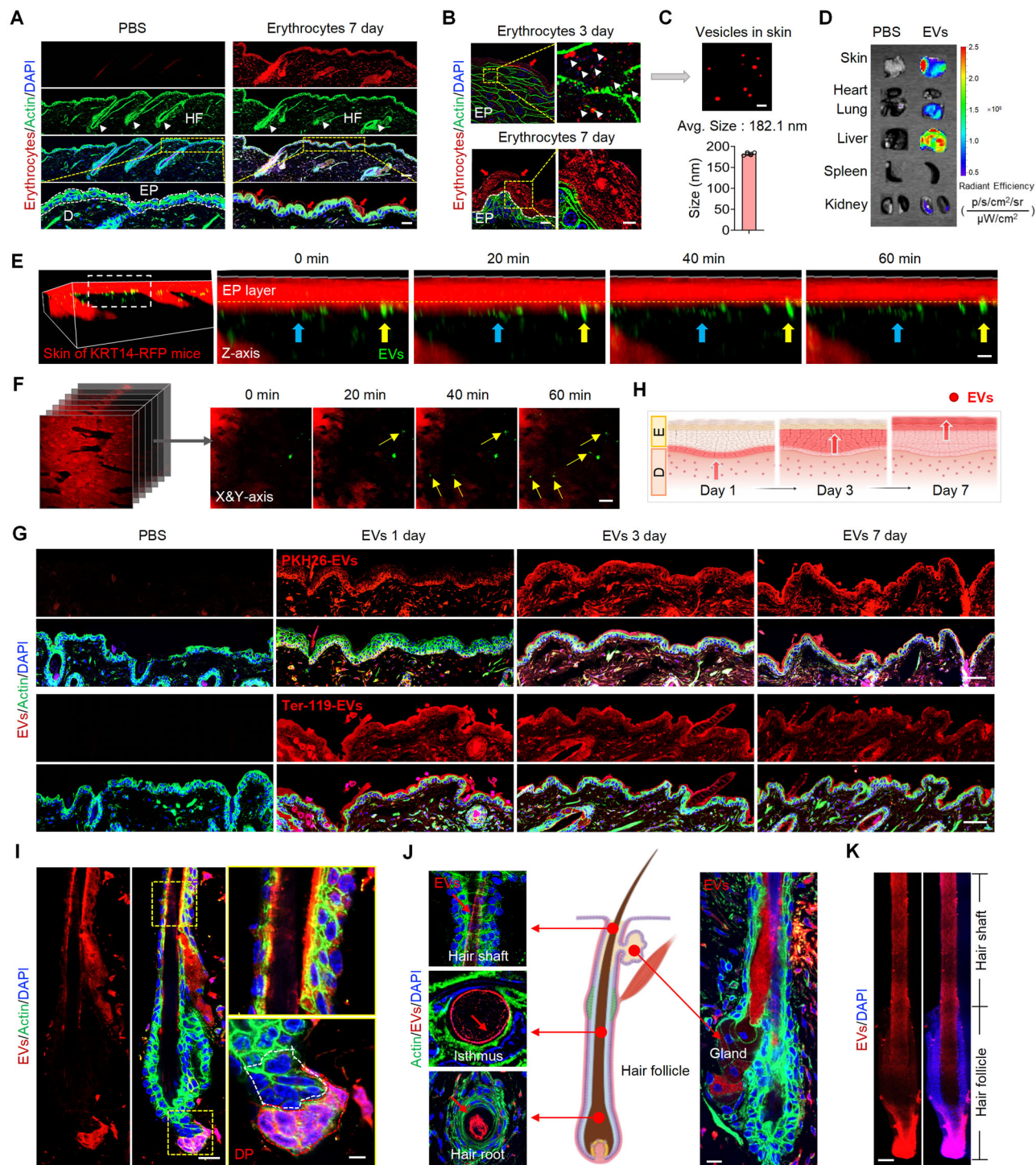


FIGURE 1 | Biodistribution profile of erythrocyte EVs in the integumentary hair and skin. (A) Distribution of PKH26-labelled erythrocytes in the skin at 7 days after tail vein injection. Scale bars, 50 μ m for lower magnification, 20 μ m for higher magnification. (B) Distribution of PKH26-labelled erythrocytes in the EP layer at 3 and 7 days after tail vein injection. Scale bars, 10 μ m for lower magnification, 5 μ m for higher magnification. (C) Extracted PKH26-positive particles in the EP layer at 3 days postinfusion assessed by SIM and NanoFCM. Scale bar, 1 μ m. (D) Biodistribution of erythrocyte EVs at 7 days after tail vein injection. (E, F) The dynamic migration of PKH67-labelled erythrocyte EVs in the epidermis of live KRT14-RFP mice. Scale bars, 1 μ m. (G) Migration of PKH26-labelled and Ter-119-labelled erythrocyte EVs in the skin. Scale bars, 50 μ m. (H) Illustration of the migration of erythrocyte EVs from inside to skin surface. (I) Distribution of erythrocyte EVs in hair follicle. Scale bars, 20 μ m. (J) Distribution of erythrocyte EVs in hair shaft, hair root and subcutaneous gland after the tail vein injection. Scale bar, 20 μ m. (K) Distribution of erythrocyte EVs in extracted hair. Scale bar, 10 μ m. DP, dermal papilla; EP, epidermal; EV, extracellular vesicle; HF, hair follicle; NanoFCM, nano-flow cytometry.

Figure 2

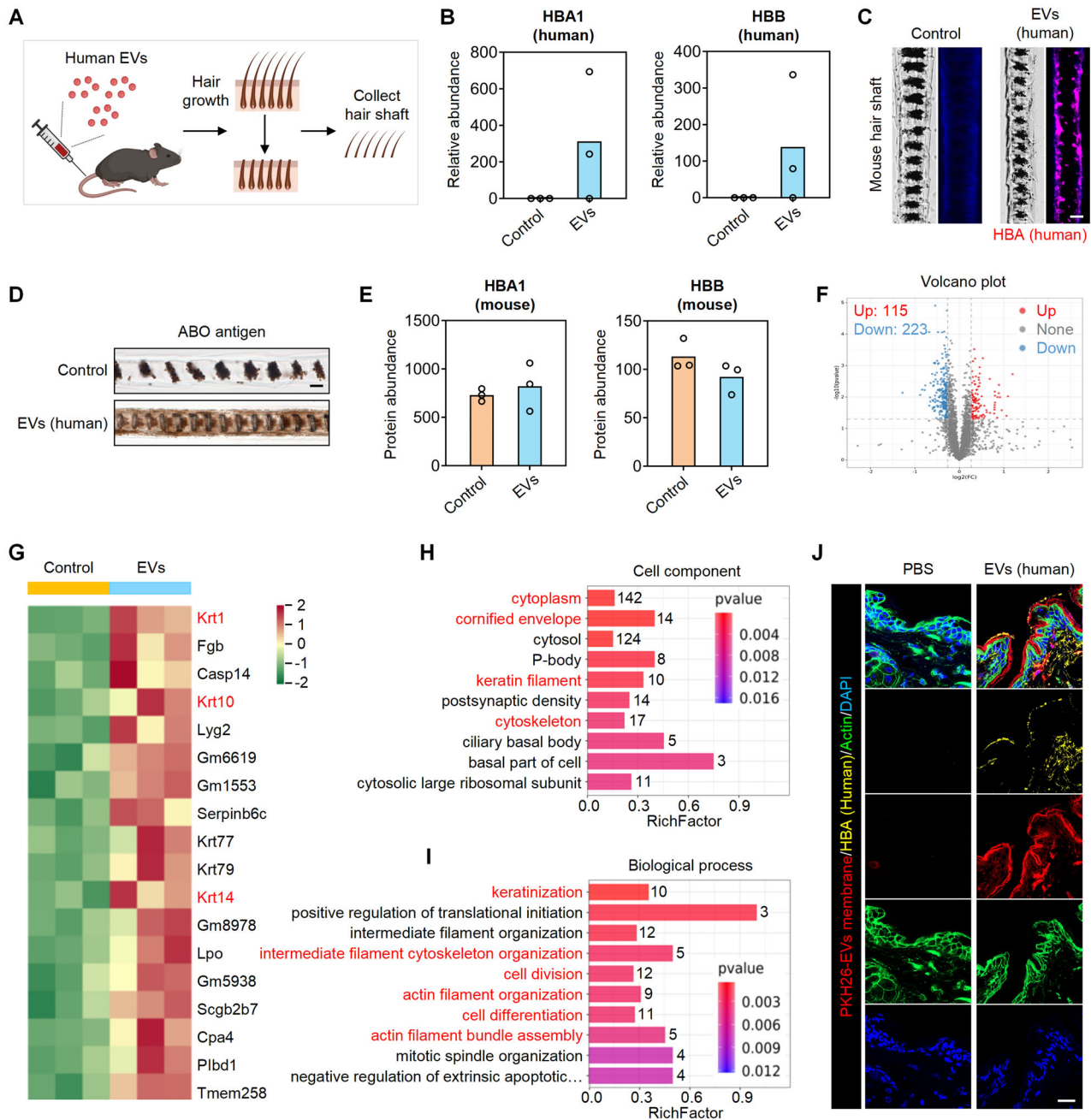


FIGURE 2 | Erythrocyte EVs are converted into hair components. (A) Illustration of hair samples from C57 mice for proteomics analysis. (B) Relative protein abundance of human HBA1 and HBB in erythrocyte EVs and control group. (C) Representative fluorescence images of the mouse hair shaft with expression of human origin HBA protein after human erythrocyte EV systematic infusion for 1 month. Scale bar, 10 μ m. (D) The expression of ABO antigens in the mouse hair shaft, as assessed by immunohistochemical staining. Scale bar, 10 μ m. (E) Proteomics analysis of the abundance of mouse HBA1 and HBB in erythrocyte EVs and control group. (F) Volcano plots showed significantly upregulated (red dots) and downregulated (blue dots) human proteins in the erythrocyte EV-treated group compared to the control group. (G) Hierarchical clustering of 115 upregulated mouse proteins (the first 18 proteins are shown here) in the erythrocyte EV group compared to the control group (Fold change > 1.2 and p value < 0.05). (H) GO cell component enrichment analysis of differentially expressed mouse proteins. (I) GO biological process enrichment analysis of differentially expressed mouse proteins. (J) The expression of human origin HBA protein in mouse skin after 7 days of PKH26-labelled human erythrocyte EV injection. Scale bar, 20 μ m. EV, extracellular vesicle; HBA, haemoglobin subunit alpha; HBB, haemoglobin subunit beta; GO, Gene Ontology.

Through detecting the HBA in mouse skin after human erythrocyte EV injection, we found that erythrocyte EV membrane and contents, such as HBA protein, ended up in multiple sites. Erythrocyte EV membrane covered skin surface in the form of a banded structure, while the most of HBA protein remained in the dermis (Figure 2J). This suggests that erythrocyte EVs may be disassembled and reorganised into different components of the skin.

3.6 | Erythrocyte EVs Contribute to Lipid Formation on the Skin Surface

Next, we analysed the lipid composition of mouse skin surface after erythrocyte EV injection (Figure 3A). Lipid content examination showed that erythrocyte EVs contained abundant Cer, phosphatidyl ethanolamine (PE), phosphatidylcholine (PC) and triglyceride (TG) (Figure 3B). Since the Cer is the main lipids that make up the EP layer (Figure 3C) (Bhattacharya et al. 2019; Pappas 2009), we speculated that erythrocyte EVs provided their membrane lipids to affect the synthesis of lipids in the EP layer. Lipidomic analysis showed that the total lipid content on the skin surface was increased in erythrocyte EV-infusion group compared with the control group (Figure 3D, E). The categories and relative proportions of lipids were nearly unchanged (Figure 3F and Figure S4A). These findings indicated that the lipid membrane of erythrocyte EVs on the skin surface was basically the same as the natural sebum membrane. Erythrocyte EVs could be a vital component for outer membrane of the skin, such as providing haemoglobin for hair growth, as well as affecting lipid synthesis including Cer, free fatty acids (FFAs), PE, phosphoacylserine (PS) and phosphatidylinositol (PI) for EP layer formation (Figure 3G). Levels of TG and cholesterol ester (CE), which have been reported as coming from sebaceous gland secretions, were not increased in erythrocyte EV-infusion group (Figure 3H). The lipid content changes in full skin layers were detected by matrix-assisted laser desorption/ionisation-time of flight mass spectrometry (MALDI-TOF-MS). The results showed that the lipids between 140 and 300 *m/z* and 500 and 800 *m/z* obviously increased in erythrocyte EV-infusion group, representing different mass of FFA and Cer, respectively (Figure 3I and Figure S4B). Combining MALDI-TOF-MS and lipidomic results, we showed that erythrocyte EVs may take part in the synthesis of some representative molecules, including FFA (10:0) (170.785 *m/z*), FFA (24:0) (366.60 *m/z*), HexCer (t20:2/18:0(2OH)) (605.224 *m/z*), PI (15:0_19:2) (833.452 *m/z*) and TG (15:0_16:0_24:0) (923.719 *m/z*) (Figure 3J). Collectively, these results demonstrate that erythrocyte EVs are integrated into the integumentary skin.

3.7 | Erythrocyte EVs Promote Hair Regeneration Through Activating Wnt/ β -Catenin Pathway

Once we revealed the amalgamation of erythrocytes and integumentary system, we further examined whether erythrocyte metabolites can regulate the function of integumentary cellular components. The results of a routine blood test and flow cytometry showed that subcutaneous injection of erythrocyte EVs had no significant influence on white blood cells (WBCs), erythrocyte, platelets (PLTs), CD4⁺, CD8⁺ or B lymphocytes (Figure S5A, B). H&E staining results also demonstrated that erythrocyte EV-

treated mice had no observable histological abnormalities of the heart, liver, spleen, lung or kidney (Figure S5C).

We next tested the effect of erythrocyte EVs on hair regeneration in C57 and Balb/c mice. Minoxidil (5%) and PBS were used as the positive and negative controls, respectively. At 7 days post-subcutaneous injection, the back skin of the mice became significantly darkened compared to its original colour in the erythrocyte EV group relative to the minoxidil group and PBS group (Figure 4A). At 10 days postinjection, the back skin was completely covered by new hair in the erythrocyte EV group and the length of newly formed hair was much longer than in the minoxidil group or the PBS group (Figure 4A, B). In Balb/c mice, subcutaneous injection of erythrocyte EVs also promoted hair follicles to quickly enter the anagen stage and promoted hair growth (Figure S6A, B). H&E staining showed that both the length and number of hair follicles in the erythrocyte EV group were significantly greater than in the minoxidil group and PBS group (Figure 4C and Figure S6C). Since Wnt/ β -catenin pathway is well known as the critical signalling network in hair regrowth, we showed that erythrocyte EVs induced substantial upregulation of Wnt/ β -catenin signalling in skin tissues after subcutaneous erythrocyte EV injection (Figure 4D).

Since it is well known that the DP plays a crucial role in hair follicle development and regeneration, mouse DPCs were isolated for further study (Figure S7A). After incubating normal mouse DPCs with erythrocyte EVs for 3 days, western blotting results showed that the erythrocyte EVs significantly increased the expression of active β -catenin, enhanced proliferation rate (Figure S7B), as well as increased osteogenic and adipogenic differentiation in DPCs (Figure S7C, D), but these effects were significantly attenuated by XAV939, an inhibitor of Wnt/ β -catenin pathway, treatment (Figure S7E). In conclusion, our experimental data reveal a previously unknown role of erythrocyte EVs in promoting hair regeneration via activating Wnt/ β -catenin signalling in DPCs.

3.8 | Erythrocyte EVs Rescue Hair and Skin Defects in Anaemic Mice

H&E staining results showed that erythrocyte EV injection increased the number of fibroblasts in the dermis layer of anaemic mice, reduced the karyopyknosis of keratinocytes in the EP layer and promoted restoration of normal EP organisation (Figure 4E). SEM imaging showed that erythrocyte EV treatment repaired the large cracks in the hair cuticles, eliminating exposure of the cortex in the hair shafts of anaemic mice (Figure 4F). After treatment with erythrocyte EVs, the hair shafts also exhibited a complete and smooth profile nearly the same as that of normal hair (Figure 4F). The immunofluorescent images showed that erythrocyte EVs activated β -catenin of hair follicle in anaemic mice, promoted DP growth and hair follicle turnover (Figure 4G). Furthermore, we showed that DPCs from anaemic mice were able to engulf erythrocyte EVs in vitro and upregulated the expression of active β -catenin as assessed by immunofluorescent staining (Figure 5A). Western blotting analysis showed that the reduced level of active β -catenin in DPCs of anaemic mice was elevated after erythrocyte EV treatment (Figure 5B). Furthermore, erythrocyte EV treatment improved proliferation rate (Figure 5C) as well as osteogenic and adipogenic differentiation of DPCs

Figure 3

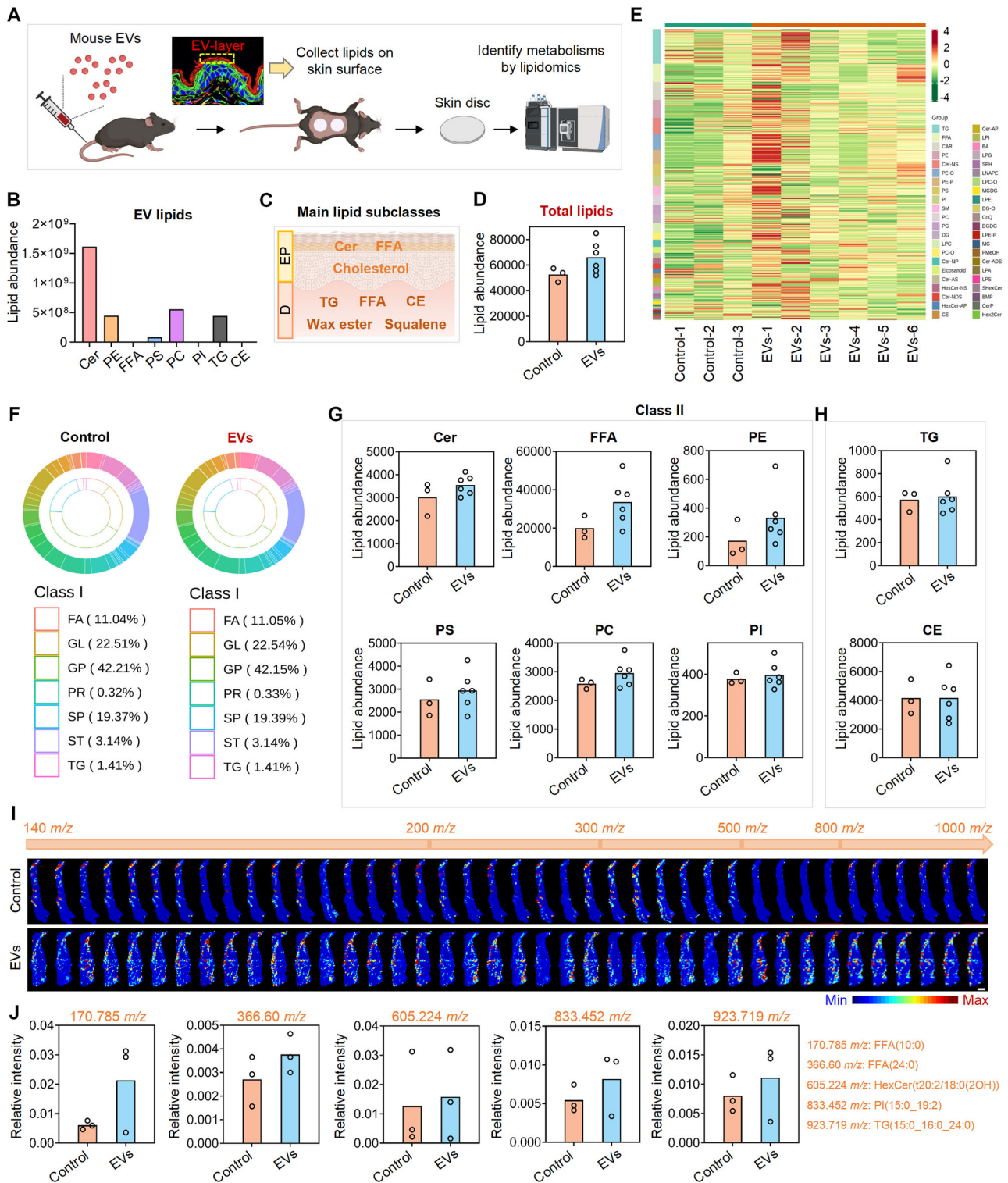


FIGURE 3 | Erythrocyte EVs contribute to the lipid formation on the skin surface. (A) Illustration of lipids on skin surface from C57 mice for lipidomic detection. (B) The content of lipids in erythrocyte EVs. (C) Illustration of main lipid subclasses in the epidermal (EP) and dermal (D) layers. (D) The content of total lipids on the skin surface of erythrocyte EV-infused and wildtype control mice. (E) Hierarchical clustering of all lipids on skin surface in erythrocyte EV-treated mice and wildtype control mice (Fold change > 1.5 and p value < 0.05). (F) Ratio of lipid classes on the skin surface of erythrocyte EV-infused and wildtype control mice. (G, H) The content of lipid subclasses on the skin surface of erythrocyte EV-infused and wildtype control mice. (I) MALDI-TOF-MS images of lipids in full skin layers of erythrocyte EV-infused and wildtype control mice. Scale bar, 300 μ m. (J) The content of representative lipids in full skin layers of erythrocyte EV-infused and wildtype control mice analysed by MALDI-TOF-MS. CE, cholesterol ester; Cer, ceramide; EV, extracellular vesicle; FA, fatty acids; FFA, free fatty acid; GL, glycerolipids; GP, glycerophospholipids; MALDI-TOF-MS, matrix-assisted laser desorption/ionisation-time of flight mass spectrometry; PC, phosphatidylcholine; PE, phosphatidyl ethanolamine; PI, phosphatidylinositol; PR, prenol lipids; PS, phosphoacylserine; SP, sphingolipids; ST, sterol lipids; TG, triglyceride.

Figure 4

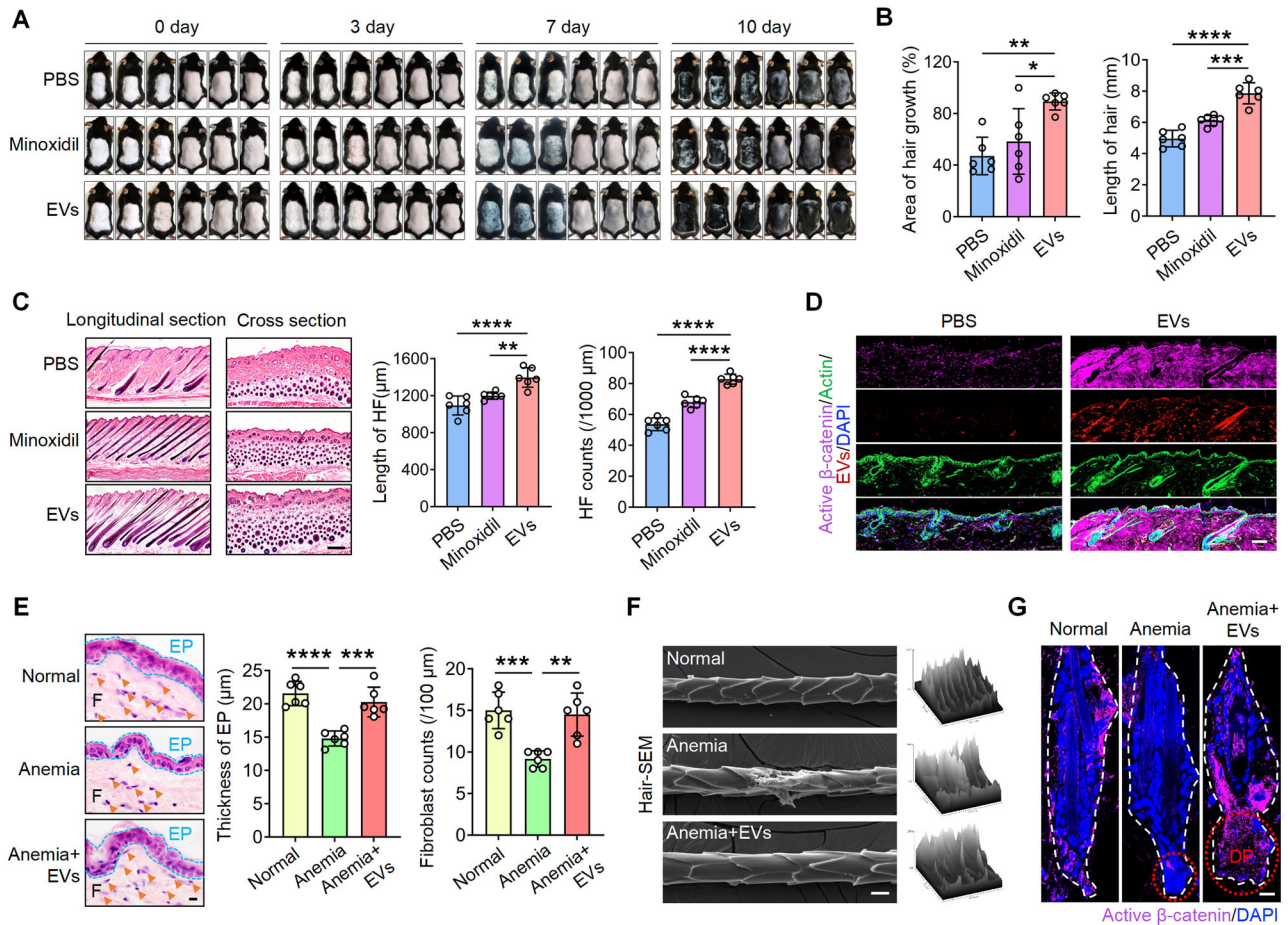


FIGURE 4 | Erythrocyte EVs promote hair regeneration in wildtype mice and rescue hair and skin defects in anaemic mice. (A) Representative photos of C57 mouse hair regrowth at 0, 3, 7 and 10 days after treatment with erythrocyte EVs. Minoxidil and PBS treatment was used as positive and negative controls, respectively ($n = 6$). (B) Relative intensity of the darkness of the back skin and hair length on day 10 postinjection in C57 mice. (C) H&E staining of longitudinal and cross sections of erythrocyte EV-treated mouse skin and the number and length of hair follicles ($n = 6$). Scale bar, 100 μm. (D) Representative fluorescence images showed the activation of Wnt/ β -catenin pathway in mouse skin tissues after subcutaneous erythrocyte EV injection for 3 days. Scale bar, 50 μm. (E) H&E staining of skin tissues in normal, anaemic and erythrocyte EV-treated anaemic mice. Scale bar, 10 μm. Thickness of epidermal (EP) layer and fibroblast counts in dermal (D) layer were analysed by ImageJ. (F) Hair microstructure in normal, anaemic and erythrocyte EV-treated anaemic mice assessed by SEM. Scale bar, 10 μm. (G) Representative fluorescence images showed the activation of Wnt/ β -catenin pathway in hair follicles of normal, anaemic and erythrocyte EV-treated anaemic mice. Scale bar, 10 μm. * $p < 0.05$, ** $p < 0.01$, *** $p < 0.001$ and **** $p < 0.0001$. EV, extracellular vesicle; PBS, phosphate buffered saline.

in anaemic mice through activating Wnt/ β -catenin pathway (Figure 5D), while these effects were counteracted by XAV939 treatment (Figure 5E, F). In conclusion, these data suggest that erythrocyte EVs have a significant therapeutic effect for the hair and skin disorders in anaemic mice.

Since it was reported that erythrocyte EVs contained abundant miRNAs (Kontidou et al. 2023), we examine whether these miRNAs contribute to the activation of Wnt/ β -catenin pathway in anaemic DPCs. Axin2 is a key negative regulatory factor of Wnt/ β -catenin pathway. We used online software, DIANA and Targetscan, to computationally search miRNA targets on Axin2 and predicted 10 miRNAs that may target Axin2 gene expression (Table S4). We used reverse transcription quantitative PCR (RT-qPCR) to reveal elevated expression of miR-20a-5p, miR-22-3p and miR-195a-5p in erythrocyte EV-treated anaemic

DPCs (Figure 5G). These miRNA mimics were used to treat DPCs and showed that miR-20a-5p, miR-22-3p and miR-195a-5p downregulated Axin2 expression, but miR-20a-5p and miR-22-3p mimics induced β -catenin accumulation in anaemic DPCs (Figure 5H). Dual-luciferase reporter gene assay showed that miR-20a-5p and miR-22-3p could bind to the promoter region of Axin2 (Figure S8A). EVs can release miR-20a-5p or miR-22-3p into the DPCs and significantly inhibit the expression of Axin2 (Figure S8B). RT-qPCR results showed that siRNA knockdown efficiently reduced the levels of miR-20a-5p and miR-22-3p in erythrocytes (Figure S8C). Western blotting analysis showed that EVs from miR-20a-5p or miR-22-3p knockdown erythrocytes failed to downregulate Axin2 and upregulate active β -catenin (Figure 5I). These data suggest that miR-20a-5p and miR-22-3p had a significant effect on the erythrocyte EV-mediated Axin2/ β -catenin cascade. Thus, we selected miR-20a-5p and miR-22-3p

Figure 5

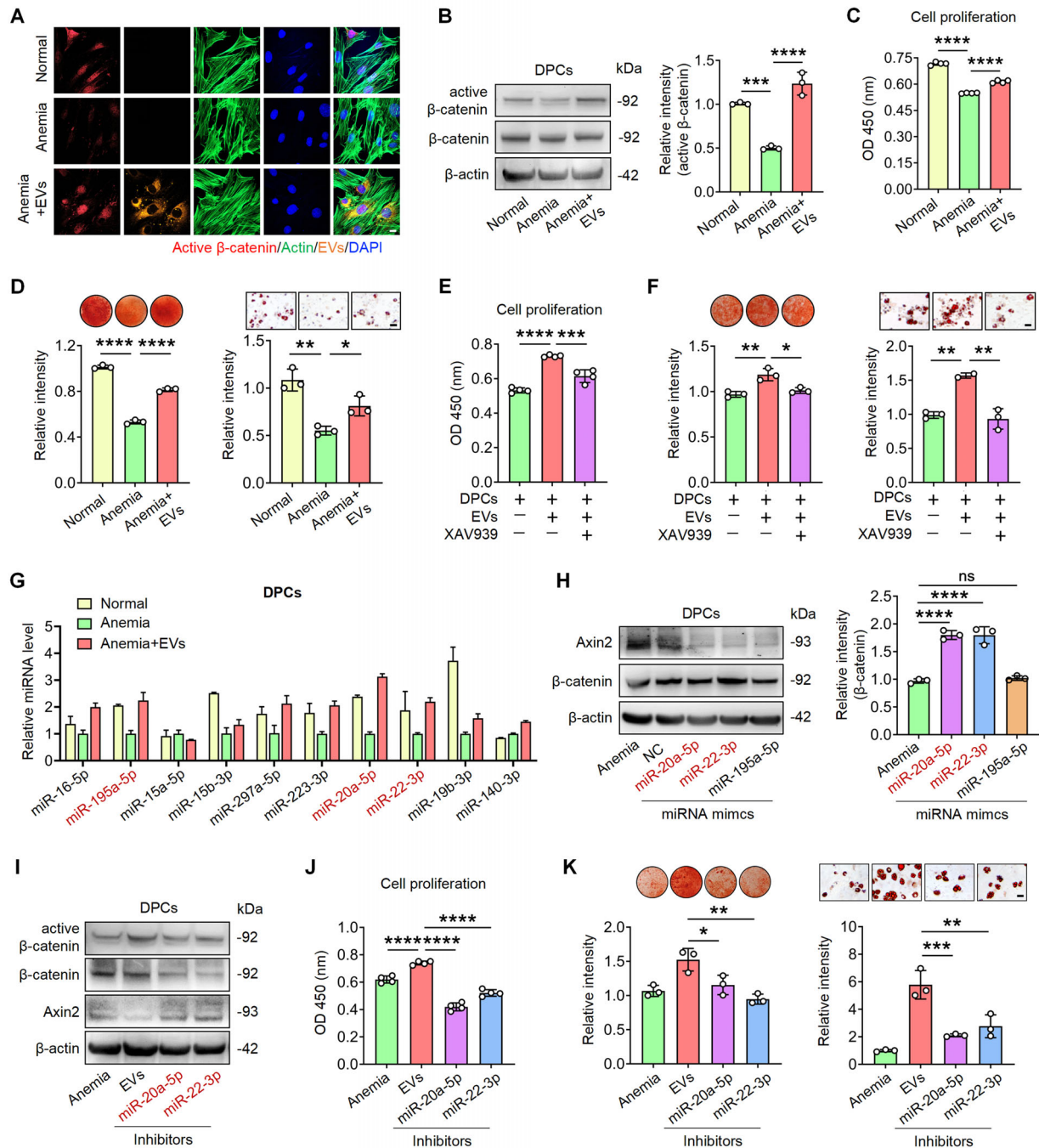


FIGURE 5 | miR-20a-5p and miR-22-3p contribute to erythrocyte EV-mediated rescue of impaired anaemic DPCs. (A) Representative images showed the activation of Wnt/ β -catenin pathway in DPCs from normal, anaemic and erythrocyte EV-treated anaemic mice. Scale bar, 10 μ m. (B) Western blotting analysis showed the expression level of Wnt/ β -catenin in anaemic DPCs after incubation with erythrocyte EVs for 3 days. (C) Proliferation ability of anaemic DPCs after incubation with erythrocyte EVs for 3 days. (D) The osteogenic and adipogenic differentiation ability of anaemic DPCs after incubation with erythrocyte EVs for 3 days. Scale bar, 50 μ m; (E) Proliferation ability of anaemic DPCs after treatment with erythrocyte EVs alone or in conjunction with XAV939 (10 μ M). (F) The osteogenic and adipogenic differentiation ability of anaemic DPCs after treatment with erythrocyte EVs alone or in conjunction with XAV939 (10 μ M). Scale bar, 50 μ m. (G) RT-qPCR analysis showed the levels of miR-20a-5p, miR-22-3p and miR-195a-5p were increased in erythrocyte EV-treated anaemic DPCs. (H) Western blotting analysis showed the expression level of Axin2 and β -catenin in anaemic DPCs after incubation with miR-20a-5p, miR-22-3p and miR-195a-5p mimics. (I) Western blotting analysis showed the expression level of Axin2 and active β -catenin in anaemic DPCs after incubation with control EVs and EVs from miR-20a-5p or miR-22-3p knockdown erythrocytes. (J) Proliferation rate of anaemic DPCs after incubation with control EVs and EVs from miR-20a-5p or miR-22-3p knockdown erythrocytes for 3 days. (K) The osteogenic and adipogenic differentiation ability of anaemic DPCs after incubation with control EVs and EVs from miR-20a-5p or miR-22-3p knockdown erythrocytes for 3 days. Scale bar, 50 μ m; * p < 0.05, ** p < 0.01, *** p < 0.001 and **** p < 0.0001. DPC, dermal papilla cell; EV, extracellular vesicle; NC, negative control; ns, not significant.

as the functional miRNAs for the following study. When DPCs from anaemic mice were treated by EVs from miR-20a-5p or miR-22-3p knockdown erythrocytes, the rescue effects were partially abolished when compared with control erythrocyte EV group in terms of proliferation, osteogenic differentiation and adipogenic differentiation (Figure S9J, K).

Erythrocyte EV treatment enhanced anaemic SMSC proliferation rate as well as osteogenic and adipogenic differentiation by activating the Wnt/ β -catenin pathway (Figure S9A–C). These effects were abolished by XAV939 treatment (Figure S9B, C). Moreover, we showed that miR-20a-5p and miR-22-3p in EVs improved anaemic SMSC function via mediating Axin2/ β -catenin cascade (Figure S9D–F). EVs from miR-20a-5p or miR-22-3p knockdown erythrocytes lost their positive effect on anaemic SMSCs, including proliferation, osteogenic and adipogenic differentiation abilities (Figure S9G, H).

3.9 | Erythrocyte EVs Promote Hair Regeneration in AGA Patients

We initiated a clinical study to evaluate the safety and effectiveness of autologous erythrocyte EVs for treating AGA. We conducted three times erythrocyte EV-injection and 6-month follow-up for nine patients (Figure 6A and Table S3). A schematic diagram of the preparation of autologous erythrocyte EVs was shown in Figure S10A. Zetaview results showed that each erythrocyte produced around 122 EVs (Figure S10B), with an average particle size of 216.6 nm and Zeta potential of -45.86 ± 1.71 mV (Figure S10B). We used macroscopic photos and TrichoScan to analyse the outcomes of erythrocyte EV treatment for AGA patients (Figure 6B and Figure S11A). There were significant increases from baseline to 6 months in both anagen hair ratio and hair density (Figure 6C, D). This indicates that erythrocyte EVs effectively promoted the transition of hair follicles into the anagen stage and stimulated hair regrowth after three local scalp injections. The density of vellus hair was significantly upregulated throughout the entire treatment and follow-up period (Figure 6E and Figure S11B). The density of terminal hairs showed a slight increase at 6 months, but without changes in hair thickness (Figure 6F, G). This suggests that autologous erythrocyte EV treatment can effectively improve hair growth in AGA patients.

4 | Discussion

There are about 1% of erythrocytes in the peripheral blood undergo natural degradation, while an equivalent proportion of erythrocytes mature in the bone marrow and are released into the circulation. Given the substantial daily turnover of erythrocytes in the body, it raises the question of where these erythrocytes ultimately eliminated. It was reported that the liver may be the primary organ responsible for clearing senescent and apoptotic erythrocytes, with its key function being the recycling of iron ions (Theurl et al. 2016). Our study revealed that skin and hair may serve as a site to excrete erythrocytes and apoptotic vesicles (Ma et al. 2023). Meanwhile, the integumentary system is also undergoing periodic renewal. However, the detailed relationship between these two systems is unclear. In our study, we showed that erythrocytes, the largest cell population in the blood, inte-

grate with the integumentary system. First, we showed that the compromised erythrocytes in anaemic mice severely affect their hair and skin. Then, we found that the integumentary system is an elimination organ through which erythrocyte EVs exit the body. Erythrocyte EVs provide copious amounts of fundamental materials such as haemoglobin and keratins that are crucial components of hair and skin structure. Finally, we demonstrated that erythrocyte EVs can significantly promote hair regeneration, rescue integumentary disorders in anaemic mice and promote hair growth in AGA patients. We suggest that the blood system and integumentary system are biologically integrated.

Haemoglobin is well known as an iron-containing protein in erythrocytes that gives blood its red colour. It has two primary functions: delivering oxygen to cells throughout the body and carrying carbon dioxide back to the lungs. Abnormal types of haemoglobin lead to impairment of the structure and function of erythrocytes, leading to devastating disorders such as sickle cell anaemia. In our study, we found that haemoglobin was involved in hair growth and incorporated into hair cortex. This led us to speculate that haemoglobin may be a protein responsible for supporting hair structure. The GO enrichment analysis of hair proteomics demonstrated that some BPs, such as keratinisation and actin filament organisation, are activated after erythrocyte EV treatment. This inspired us to explore whether the haemoglobin in erythrocyte EVs play a role in EP keratinisation. Recently, a study revealed that HBA, which is only expressed in keratinised stratified squamous epithelium, acts as an antioxidant, contributing to skin barrier function (Tahara et al. 2023). Our study further emphasises the nonnegligible role of haemoglobin in the integumentary system.

Hair loss can be a natural process. About 50–100 hairs fall out of the human head every day, providing a biological resource that can be used in DNA analysis, protein analysis and ABO blood group typing (Miyasaka et al. 1987; Nishi et al. 1989). Remarkably, proteomic analysis can be performed even on hair shafts only 1 mm in length (Liu et al. 2023). In our study, we found that erythrocyte EVs are a major element in the hair, building the structure of the hair shafts by providing significant quantities of structural proteins such as haemoglobin, keratin 1, keratin 10 and keratin 14. It is therefore possible to consider erythrocytes a part of the integumentary system.

According to our previous study (Ma et al. 2023), we found that mechanical force regulated the metabolism and migration of EVs through Wnt/ β -catenin pathway in the skin. In this study, we showed that subcutaneous injection of erythrocyte EVs upregulated Wnt/ β -catenin expression in the skin (Figure 4D), which may regulate erythrocyte EV migration and play a critical role in skin and hair regeneration. It is true that the endosomal entrapment can prevent efficient cargo delivery to the cytoplasm and, therefore, reduce the effectiveness of miRNA-based therapies (Zhang et al. 2015). Recent studies have shown that erythrocyte EVs contain abundant miRNAs inherited from erythrocytes (Kong et al. 2021; Kontidou et al. 2023; Sun et al. 2020) and are capable of transporting miRNAs to recipient cells to have regulating effects (Regev-Rudzki et al. 2013; Thangaraju et al. 2020; Wang et al. 2017). In our study, we showed that miRNAs from erythrocyte EVs activated Wnt/ β -catenin pathway to promote DPC function and hair regeneration. In addition,

Figure 6

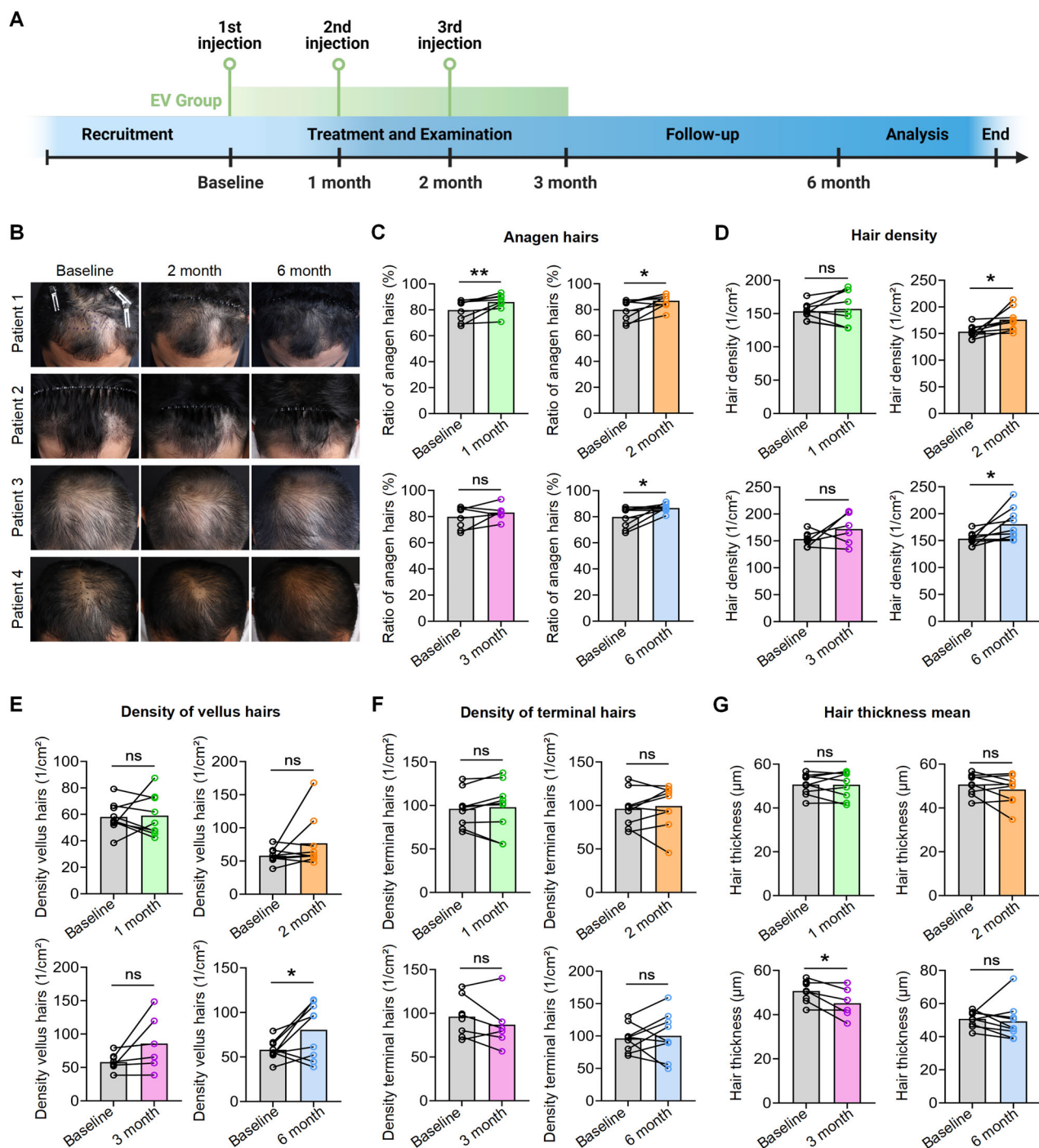


FIGURE 6 | Erythrocyte EVs promote hair regeneration in AGA patients. (A) Illustration of clinical trial schedule. (B) Representative photographs of improvement in AGA patients after erythrocyte EV treatment at baseline (preinjection), 2 and 6 months (postinjection). (C–G) Changes of anagen hair ratio, hair density, vellus hair density, terminal hair density and hair thickness mean from baseline (preinjection) to 1, 2, 3 and 6 months (postinjection) assessed by TrichoScan analysis. Data were analysed using paired two-tailed Student's *t* tests. **p* < 0.05, ***p* < 0.01 and ns, not significant. AGA, androgenic alopecia; EV, extracellular vesicle.

protein is also considered an important EV cargo for regulatory effects. We have searched the protein expression profiles of erythrocyte EVs and screened some proteins that may be related to hair growth (Table S5). We will further explore the role of these proteins in hair and skin repairment.

It is widely known that the EP layer is an important natural barrier against various types of environmental damages, including those affected by bacteria and ultraviolet radiation. The sebum membrane is a lipid layer that forms the outmost covering of the epidermis, itself the outmost layer of the skin with the important

task of protecting the body. We show that erythrocyte EVs form this crucial first lipid barrier on the skin surface, and that the composition of these EVs is almost the same as that of the natural sebum membrane. It has been reported that the lipids secreted by the sebaceous glands include TGs, wax esters, FFAs, squalene, CE and cholesterol (Pappas 2009). The lipids in the EP layer primarily consist of Cers and phospholipids, which are not found in the sebaceous glands. Among these, Cers are key components involved in the formation of the EP barrier (Bhattacharya et al. 2019). In this study, we showed that lipid components such as Cers, FFAs and PE were increased after intravenous injection of erythrocyte EVs. Due to the abundant quantity of erythrocytes in the body, erythrocyte EVs may play a crucial role to form lipid barrier on skin surface.

Our study has proposed a new viewpoint that erythrocytes from blood system are integrated with the integumentary system and play critical roles to maintain homeostasis of the integumentary system. The results of the clinical study indicate that erythrocyte EV injection is an effective treatment for AGA patients.

Author Contributions

Songtao Shi: Conceptualization (lead), funding acquisition (lead), project administration (lead), resources (lead), writing – original draft (lead). **Zeyuan Cao:** Conceptualization (equal), data curation (lead), formal analysis (lead), investigation (lead), methodology (lead), project administration (lead), writing – original draft (lead). **Peiyi Li:** Data curation (supporting), investigation (supporting), methodology (supporting), project administration (supporting), writing – original draft (supporting). **Manjin Zhang:** Investigation (supporting), methodology (supporting), project administration (supporting), writing – original draft (supporting). **Simin Cai:** Methodology (supporting), project administration (supporting), resources (supporting), writing – original draft (supporting). **Na Li:** Data curation (supporting), methodology (supporting), resources (supporting). **Mingtao Luo:** Data curation (supporting), methodology (supporting), resources (supporting). **Yinghui Li:** Investigation (supporting), methodology (supporting), resources (supporting). **Haolin Wu:** Methodology (supporting), resources (supporting). **Xueli Mao:** Funding acquisition (supporting), resources (supporting). **Ruibao Ren:** Methodology (supporting), project administration (supporting), resources (supporting). **Hongju Xie:** Data curation (equal), funding acquisition (supporting), project administration (supporting), resources (supporting), validation (equal).

Acknowledgements

The authors thank the grants from the National Key Research and Development Program of China (2021YFA1100600 to S.S., 2022YFA104402 to X.M.), Pearl River Talent Recruitment Program (2019ZT08Y485, 2019JC01Y182 to S.S.), Hainan Health and Medical Technology Innovation Joint Project (WSJK2024MS152 to H.X.) and Hainan Provincial Higher Education Scientific Research Project (Hnky2021ZD-16 to H.X.) for the support.

Conflicts of Interest

Songtao Shi and Zeyuan Cao are listed as an inventor on the patents (Application number: CN202210625524.4, CN202210624896.5) related to the research described in this manuscript. The other authors declare no conflicts of interest.

Data Availability Statement

The data that support the findings of this study are available from the corresponding author upon reasonable request.

References

- Armutcu, F. 2019. “Organ Crosstalk: The Potent Roles of Inflammation and Fibrotic Changes in the Course of Organ Interactions.” *Inflammation Research* 68: 825.
- Bhattacharya, N., W. J. Sato, A. Kelly, G. Ganguli-Indra, and A. K. Indra. 2019. “Epidermal Lipids: Key Mediators of Atopic Dermatitis Pathogenesis.” *Trends in Molecular Medicine* 25: 551–562.
- Bianconi, E., A. Piovesan, F. Facchin, et al. 2013. “An Estimation of the Number of Cells in the Human Body.” *Annals of Human Biology* 40: 463.
- Bruce, A. J., T. P. Pincelli, M. G. Heckman, et al. 2020. “A Randomized, Controlled Pilot Trial Comparing Platelet-Rich Plasma to Topical Minoxidil Foam for Treatment of Androgenic Alopecia in Women.” *Dermatologic Surgery* 46: 826–832.
- Castillo-Armengol, J., L. Fajas, and I. C. Lopez-Mejia. 2019. “Inter-Organ Communication: A Gatekeeper for Metabolic Health.” *EMBO Reports* 20: e47903.
- Grubauer, G., K. R. Feingold, and P. M. Elias. 1987. “Relationship of Epidermal Lipogenesis to Cutaneous Barrier Function.” *Journal of Lipid Research* 28: 746.
- Harris-Tryon, T. A., and E. A. Grice. 2022. “Microbiota and Maintenance of Skin Barrier Function.” *Science* 376: 940.
- Herrlich, A., E. Kefaloyianni, and S. Rose-John. 2022. “Mechanisms of Interorgan Crosstalk in Health and Disease.” *FEBS Letters* 596: 529.
- Kim, S. J., M. J. Kim, Y. J. Lee, et al. 2021. “Innovative Method of Alopecia Treatment by Autologous Adipose-Derived SVF.” *Stem Cell Research & Therapy* 12: 486.
- Kong, Y., X. Tian, R. He, et al. 2021. “The Accumulation of Exosome-Associated microRNA-1246 and microRNA-150-3p in Human Red Blood Cell Suspensions.” *Journal of Translational Medicine* 19: 225.
- Kontidou, E., A. Collado, J. Pernow, and Z. Zhou. 2023. “Erythrocyte-Derived microRNAs: Emerging Players in Cardiovascular and Metabolic Disease.” *Arteriosclerosis, Thrombosis, and Vascular Biology* 43: 628–636.
- Lam, L., S. Murphy, D. Kokkinaki, et al. 2021. “DNA Binding to TLR9 Expressed by Red Blood Cells Promotes Innate Immune Activation and Anemia.” *Science Translational Medicine* 13: j1008.
- Lee, W.-S., B. I. Ro, S. P. Hong, et al. 2007. “A New Classification of Pattern Hair Loss That Is Universal for Men and Women: Basic and Specific (BASP) Classification.” *Journal of the American Academy of Dermatology* 57: 37–46.
- Liu, Z., H. Simayijiang, Q. Wang, et al. 2023. “DNA and Protein Analyses of Hair in Forensic Genetics.” *International Journal of Legal Medicine* 137: 613–633.
- Lopez, A., P. Cacoub, I. C. Macdougall, and L. Peyrin-Biroulet. 2016. “Iron Deficiency Anaemia.” *Lancet* 387: 907.
- Ma, L., C. Chen, D. Liu, et al. 2023. “Apoptotic Extracellular Vesicles Are Metabolized Regulators Nurturing the Skin and Hair.” *Bioactive Materials* 19: 626.
- Miyasaka, S., M. Yoshino, H. Sato, B. Miyake, and S. Seta. 1987. “The ABO Blood Grouping of a Minute Hair Sample by the Immunohistochemical Technique.” *Forensic Science International* 34: 85–98.
- Nishi, K., B. Annuss, S. Rand, and B. Brinkmann. 1989. “ABO Blood Grouping of Hairs Using an Avidin-Biotin-Peroxidase Complex Technique.” *Zeitschrift Fur Rechtsmedizin* 102: 247.
- Pappas, A. 2009. “Epidermal Surface Lipids.” *Dermatoendocrinology* 1: 72–76.

- Pasini, E. M., H. U. Lutz, M. Mann, and A. W. Thomas. 2010. "Red Blood Cell (RBC) Membrane Proteomics—Part I: Proteomics and RBC Physiology." *Journal of Proteomics* 73: 403.
- Piraccini, B. M., and A. Alessandrini. 2014. "Androgenetic Alopecia." *Giornale Italiano Di Dermatologia E Venereologia* 149: 15.
- Regev-Rudzki, N., D. W. Wilson, T. G. Carvalho, et al. 2013. "Cell-Cell Communication Between Malaria-Infected Red Blood Cells via Exosome-Like Vesicles." *Cell* 153: 1120–1133.
- Saceda-Corrado, D., M. Domínguez-Santas, S. Vañó-Galván, and R. Grimalt. 2023. "What's New in Therapy for Male Androgenetic Alopecia?" *American Journal of Clinical Dermatology* 24: 15–24.
- Sender, R., S. Fuchs, and R. Milo. 2016. "Revised Estimates for the Number of Human and Bacteria Cells in the Body." *PLoS Biology* 14: e1002533.
- Sun, L., Y. Yu, B. Niu, and D. Wang. 2020. "Red Blood Cells as Potential Repositories of MicroRNAs in the Circulatory System." *Frontiers in Genetics* 11: 442.
- Tahara, U., T. Matsui, T. Atsugi, et al. 2023. "Keratinocytes of the Upper Epidermis and Isthmus of Hair Follicles Express Hemoglobin mRNA and Protein." *Journal of Investigative Dermatology* 143: 2346–2355.e10.
- Thangaraju, K., S. N. Neerukonda, U. Katneni, and P. W. Buehler. 2020. "Extracellular Vesicles From Red Blood Cells and Their Evolving Roles in Health, Coagulopathy and Therapy." *International Journal of Molecular Sciences* 22: 153.
- Theurl, I., I. Hilgendorf, M. Nairz, et al. 2016. "On-Demand Erythrocyte Disposal and Iron Recycling Requires Transient Macrophages in the Liver." *Nature Medicine* 22: 945–951.
- Varothai, S., and W. F. Bergfeld. 2014. "Androgenetic Alopecia: An Evidence-Based Treatment Update." *American Journal of Clinical Dermatology* 15: 217.
- Vorselen, D., S. M. Van Dommelen, R. Sorkin, et al. 2018. "The Fluid Membrane Determines Mechanics of Erythrocyte Extracellular Vesicles and Is Softened in Hereditary Spherocytosis." *Nature Communications* 9: 4960.
- Wang, Z., J. Xi, X. Hao, et al. 2017. "Red Blood Cells Release Microparticles Containing human Argonaute 2 and miRNAs to Target Genes of Plasmodium Falciparum." *Emerging Microbes & Infections* 6: 1–11.
- Zhang, J., S. Li, L. Li, et al. 2015. "Exosome and Exosomal microRNA: Trafficking, Sorting, and Function." *Genomics, Proteomics & Bioinformatics* 13: 17–24.

Supporting Information

Additional supporting information can be found online in the Supporting Information section.